Thermodynamic Properties of Hydrogen-Water Adsorption at terraces and steps of Pt(111) Vicinal Surface Electrodes

Ana M. Gómez–Marín*[a,b] and Juan M. Feliu*[a]

[a]*Instituto de Electroquímica, Universidad de Alicante, Apt 99, E-03080 Alicante, Spain, Tel.: +34 965 909 301; fax: +34 965 903 537. Email: juan.feliu@ua.es (J.M. Feliu), am.gomez@ua.edu.co (AM Gomez).*

[b]*Eco-Lavka, Cra. 79, #49[a]-30, Medellín, Colombia.*

Abstract:

In this work, the effect of the temperature on the adsorption states of Pt(111) vicinal surface electrodes in perchloric acid is studied through a thermodynamic analysis. The method allows calculating thermodynamic properties of the interface. In this framework, the concept of the generalized isotherm and the statistical thermodynamics description are applied to calculate formal entropies, enthalpies and Gibbs energies, $\Delta\overline{G}_i^0$, of the adsorption processes at two-dimensional terraces and one-dimensional steps. These values are compared with data from literature. Additionally, the effect of the step density on$\Delta\overline{G}_i^0$ and on the lateral interactions between adsorbed species, ω_{ij}, at terraces and steps is also determined. Calculated $\Delta\overline{G}_i^0$, entropies and enthalpies are almost temperature-independent, especially at steps, but they depend on the step orientation. In contrast, $\Delta\overline{G}_i^0$ and ω_{ij} at terraces depend on the step density, following a linear tendency for terrace lengths larger than 5 atoms. However, while $\Delta\overline{G}_i^0$ increases with the step density, ω_{ij} decreases. Results were explaining by considering the modification in the energetic surface balance by hydrogen, H_{ads}, and water, H_2O_{ads}, co-adsorption on the electrode, which in turn determines the whole adsorption processes on terraces and steps.

Keywords: Hydrogen adsorption, free Gibbs energy, stepped surfaces, thermodynamic analysis, step density, temperature analysis, cyclic voltammetry.

1. Introduction

Electrocatalytic evolution (HER) and oxidation (HOR) of hydrogen are pivotal reactions in electrochemistry, both fundamentally and technologically, because of their relevance in important processes such water splitting/formation. During these reactions in the electrode surface, hydrogen, water and other species closely interact with surface sites of the electrode material and their properties are strongly interrelated. In fact, since first studies the involvement of adsorbed hydrogen, H_{ads}, in the HER mechanism [1,2], and possibly in the

HOR [3] has been widely accepted and hence, the adsorption of hydrogen on metal surfaces has been a topic widely discussed in the literature, particularly at noble metals such as platinum [4–8].

Catalytic surfaces have a complex geometry, containing low coordination or defect sites, together with (111) terraces, and this surface heterogeneity makes difficult to extract reliable data about reaction mechanisms from electrochemical studies involving these surfaces, taking into account that the proportion between different sites on the surface depends on the particle size and shape of the catalyst[9]. Indeed, for many electrochemical reactions, defects sites are often thought to be the most active sites for catalytic reactions involving bond breaking and making steps [10].

To gain more insight into the catalytic activity at platinum surfaces, Pt single crystals can be considered as suitable models. In these surfaces, the {111} facet is modeled by a Pt(111) surface, and defect sites by its vicinal surfaces: regularly stepped single crystal surfaces with different terrace lengths, allowing the introduction of defects in a controlled approach. Two different step sites can be distinguished: those with {100} geometry and those with {110} geometry. Therefore, the study of the influence of steps, with different orientation, upon the electrochemical reactivity has become a relevant area [11–25].However, the understanding at microscopic scale of phenomena underneath voltammetric profiles, the distinction among different processes that could contribute to the voltammetric features and their dependence on various experimental parameters, is still far from being complete, and more work is still necessary to fully understand these simple signatures. In this sense, temperature dependence analysis of voltammetric profiles provides unique information about the electrochemical interface.

First studies on the temperature dependence of the hydrogen adsorption process on polycrystalline [4,5] and low index single crystal [6–8] platinum electrodes employed concepts from the thermodynamic description of electrochemical cells, and introduced the concept of a generalized isotherm into the analysis to estimate thermodynamic properties of adsorption processes at metal/interfaces. Later, works employing more precise methods to characterize the interface, like the analysis based on the electrocapillary equation [20,21,24], reported a good agreement with results from the generalized isotherm strategy [15,17].

In this paper, the temperature dependence of voltammetric profiles of stepped platinum electrodes, in contact with non-adsorbing electrolytes, is studied, and thermodynamic properties of the interface at low potentials are calculated. In this thermodynamic analysis, the generalized isotherm concept is applied to study the adsorption at both, two-dimensional terraces and one-dimensional steps. Additionally, the adsorption at steps

is also analyzed by employing the exact solution for the one-dimensional adsorption from the statistical thermodynamics description [26].

2. Experimental

Pt(111) electrodes and its vicinal surfaces, belonging to the series Pt(s)[(*n*-1)(111)x(110)] ≡Pt(s)[*n*(111)x(111)]) and Pt(s)[*n*(111)x(100)] were prepared from small Pt beads, approximately 2–3 mm in diameter, by the method described by Clavilier *et al.*[27]. All the experiments were performed in a two-compartment, three-electrode all-glass cell following a well established experimental protocol [28]. The electrochemical cell was immersed in a water bath whose temperature was controlled within ±0.1 K by a thermostat (Haake FK). The temperature in the water bath was measured with a platinum resistance thermometer (0.1 K, Crison 638Pt). The experiments were carried out at different temperatures in the range 283 K ≤ T ≤ 333 K. Prior to each experiment, the electrodes were flame-annealed, cooled in a H_2/Ar. atmosphere, and transferred to the cell protected by a drop of ultrapure water saturated with H_2/Ar. Supra-pure perchloric acid (Merck) was used to prepare the solutions in ultrapure water (Purelab Ultra, 18.2 MΩ cm, Elga-Vivendi). H_2 and Ar. (N50, Air Liquid) were also employed. All potentials were measured against the Reversible Hydrogen Electrode (RHE), immersed in the same solution and at the same temperature as the working electrode (*i.e.* the so-called isothermal configuration), a large, flame-cleaned, Pt wire coil (99.99%) was used as a counter electrode, and each experiment was repeated at least three times, with consistent results. All voltammetric scans were collected at a sweep rate of 50 mV s^{-1} at freshly annealed surfaces, and cycled first in the low potential region to verify their quality, as well as the cleanliness of the surface. The stability of the voltammetric profiles with time was also carefully checked to ensure solution cleanliness.

3. Results and discussion

Stepped surfaces are characterized by a step orientation, a terrace orientation and a terrace width. Therefore, surfaces vicinal to {111} plane are composed by close-packed {111} terraces of width equal to (*n-1*) or *n* atoms, separated by regular intervals of well-defined monoatomic steps with{110} ≡ {111}x{111} orientation, Pt(s)[(*n*-1)(111)x(110)] ≡Pt(s)[*n*(111)x(111)]), or with {100} orientation, Pt(S)[*n*(111)x(100)] [11,12,14]. Figure 1 shows positive-going voltammetric scans of Pt(776) (or Pt(s)[14(111) x(111)] ≡Pt(s)[13(111) x(110)]) and Pt(544) (or Pt(s)[9(111)x(100)]) in 0.1 M perchloric acid at 50 mV s^{-1}, at selected temperatures. In these experiments, the so-called isothermal configuration is employed, *i.e.* the RHE reference electrode is kept at the same temperature as the working electrode to avoid the formation of thermo-diffusion

potentials.

Negative counterparts of voltammetric scans presented in Fig. 1 are completely symmetrical with respect to the *x*-axis, as corresponds to a reversible adsorption dynamics, only at low potentials (E < 0.5 V). Thus, the thermodynamic analysis in this work will be devoted to this region. As seen, cyclic voltammetric profiles (CV) for stepped surfaces vicinal to the {111} plane in non-adsorbing electrolytes, within the temperature range 283.15 to 333.15 K, are quite similar to each other, and only subtle changes are seen in the CV, especially in the low potential region. For this reason, the analysis of temperature effects in this latter region should be made with great caution.

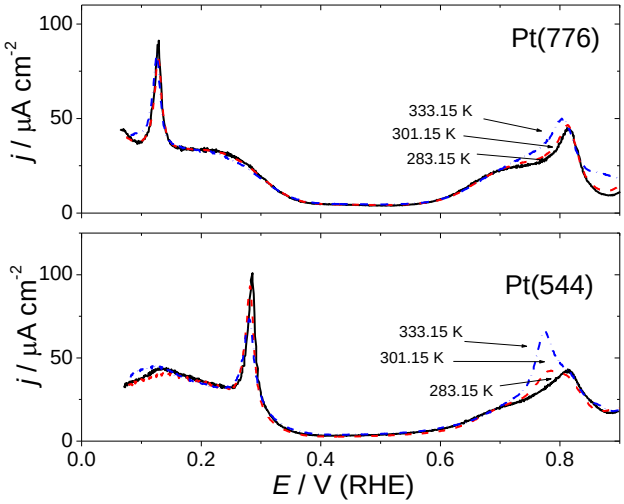

Fig. 1. Positive-going scans of cyclic voltammograms for Pt(776) and Pt(544) electrodes in 0.1 M $HClO_4$, at selected temperatures, as indicated. Scan rate 50 mVs^{-1}.

CVs in Fig. 1 are characterized by three distinctive potential regions. At E ≤ 0.35 V, hydrogen adsorption, H_{ads}, on {111} terraces is responsible for the broad pseudo-capacitive currents, while well-ordered monatomic steps give characteristic peak contributions at 0.13 V, for {110} steps, and 0.28 V vs. RHE, for {100} steps, although their origin is not entirely clear [11–14,29,30]. Steps of {110} orientation can also be seen as {111} steps, but the {110} notation is preferred because the voltammetric peak resembles that one for H_{ads} at the Pt(110) basal plane [13]. At higher potentials, between 0.6 and 0.85 V, the voltammetric charge is attributed to hydroxyl formation, OH_{ads}, from water dissociation, certainly on {111} terraces [19,23,25], but also possibly to step oxidation, although OH_{ads} and O_{ads} adsorption potentials on steps still are under controversy [23,31]. Theoretical and experimental results have suggested that OH_{ads} is less stable at steps than at terraces, because of the lack of a stable H_2O_{ads}/OH_{ads} network, while O_{ads} could adsorb on steps at lower potentials than on terraces [31, 32]. Connecting the H_{ads} and OH_{ads} regions, an apparent double layer region exists, where the current density is small, but not constant.

As mentioned, the exact origin of the sharp peaks seen in the cyclic voltammogram (CV) of stepped surfaces at low potentials is unknown. Commonly, they have been attributed to H_{ads} on step sites [11,12,14], because peak potentials are constant and charge densities linearly increase with step density, in good agreement with a process where one electron is exchanged per step atom [11–14]. However, because of their unusual pH-dependent shift of 50 mV NHE/pH unit[22,33], and their sharp shape, which can be only modeled by assuming net attractive interactions between adsorbed species [30] in contrast to repulsive H_{ads} lateral interactions on {111} terraces [15,17,20,24], it has been recently also suggested that these peaks at 0.13V and 0.28 V could be caused by competitive co-adsorption of OH_{ads}, or even adsorbed oxygen, O_{ads}, from water dissociation at steps, through a more complex reaction scheme [33]:

$$H_{ads} + [x + y]H_2O \rightleftarrows xO_{ads} + yOH_{ads} + [2x + y + 1]H^+ + [2x + y + 1]e^- (1)$$

This is because narrow and sharp peaks only appear on CVs under conditions of attractive intraparticle interactions [34], or during competitive co-adsorption of interacting molecules with high adsorption energies [35]. In Eq. (1), the peak potential (on RHE scale) may in principle depend on pH if the ratio of O_{ads}/OH_{ads} would depend on pH in a non-trivial way [33]. Nevertheless, a more simple reaction scheme, explicitly considering modifications in the double layer triggered by H_{ads} adsorption, owing to possible changes in the inner layer of chemisorbed water, H_2O_{ads}, could also explain the pH-dependence and the sharpness of these peaks, as discussed below:

$$H_{ads} + H_2O^1_{ads} \rightleftarrows H_2O^2_{ads} + H^+ + e^- (2)$$

In this scheme notations $H_2O^1_{ads}$ and $H_2O^2_{ads}$ are used just to indicate changes in the water adlayer structure before and after the adsorption of hydrogen, because of interactions between H_{ads} and H_2O_{ads} with, or without, desorption of water molecules. This is because, although solvent substitution by adsorbates is not usually considered in electrosorption processes [36], the interaction between H_{ads} and the H_2O_{ads} network already adsorbed on the electrode may strongly modify the energetic balance on the surface, which in turn may affect the whole adsorption process [31]. In this sense, results from temperature programmed desorption (TPD) experiments on Pt(111) and vicinal surfaces have shown that pre-adsorption of hydrogen, or deuterium, atoms on Pt(111) causes a stabilization of the adsorbed water on the electrode [37–41], together with a small decrease in the H_2O_{ads} coverage. Conversely, on {111} vicinal surfaces it weakens the H_2O–metal bonding at {110} and {100} steps and, at high coverages, also at {111} terraces [37,42–44]. In contrast, pre-adsorption of hydrogen on Pt(100) destabilizes the adsorbed water [45].

3.1 Thermodynamic analysis of temperature effects in the low potential region adsorption processes

Temperature effects on interfacial processes taking place at metal/solution interfaces can be well characterized by the application of a generalized isotherm, which allows determining thermodynamic properties of the global reaction of the electrochemical cell [4–6]. This is a simple, but efficient, method to estimate metal/solution thermodynamic properties of adsorption processes at Pt single crystals, in good agreement with other more precise methods, like the analysis based on the electrocapillary equation [20,21].Despite several of its implicit approximations, such as the assumption of the separability of a Langmuirian configurational term from the adsorbate chemical potential, the charge number in the adsorption process is equal to the charge of the adsorbing species in solution and the calculation of species coverages by integration of voltammograms at different temperatures, arbitrarily double-layer charging corrected. The full derivation of the mathematical expressions in this scheme has been already described in detail, and so, only main equations will be given here [15,17,20,21].

For the single adsorption of hydrogen, the half-cell reaction is given by:

$$H^+ + e^- \rightleftarrows H_{ads} \quad (3)$$

and because the RHE electrode is employed here, the half-cell reaction on the reference electrode is:

$$1/2H_2 \rightleftarrows H^+ + e^- \quad (4)$$

Then, the global reaction of the electrochemical cell is:

$$1/2H_2 \rightleftarrows H_{ads} \quad (5)$$

Application of thermodynamic equilibrium conditions to these half-cell reactions [17, 20], leads to the mean-field expression for the adsorption on two-dimensional terraces, also known as the generalized isotherm [4–6]:

$$\frac{\theta_{H_{ads}}}{1-\theta_{H_{ads}}} = exp\left(\frac{-\Delta\overline{G}^{f}_{H_{ads},Global} - FE_{RHE}}{RT}\right) \quad (6)$$

$$\Delta\overline{G}^{f}_{H_{ads},Global} = -FE_{RHE} - RTln\left(\frac{\theta_{H_{ads}}}{1-\theta_{H_{ads}}}\right) \quad (7)$$

where $\theta_{H_{ads}}$ is the potential-dependent coverage of hydrogen adsorbed on the surface, E_{RHE} is the electrode potentials vs. RHE, F is the Faraday constant, R is the ideal gas constant, T is the temperature and $\Delta\overline{G}^{f}_{H_{ads},Global}$ is the formal, coverage-dependent, standard Gibbs energy, given by:

$$\Delta\overline{G}^{f}_{H_{ads},Global} = \Delta\overline{G}^{0}_{H_{ads},Global} + \omega_{H_{ads}-H_{ads}}\theta_{H_{ads}} \quad (8)$$

with $\Delta\overline{G}^{0}_{H_{ads},Global}$, the standard molar Gibbs energy of adsorption and$\omega_{H_{ads}-H_{ads}}$, a Frumkin-type lateral interaction parameter.

In the case of adsorption in one-dimensional steps, the exact solution for the statistical thermodynamics description is known, and it is given by [26]:

$$\frac{\beta-1+2\theta_{H_{ads}}}{\beta+1-2\theta_{H_{ads}}} = exp(\frac{-\Delta\overline{G}^{f}_{H_{ads},Global}-FE_{RHE}}{RT})(9)$$

$$\Delta\overline{G}^{f}_{H_{ads},Global} = -FE_{RHE} - RTln(\frac{\beta-1+2\theta_{H_{ads}}}{\beta+1-2\theta_{H_{ads}}})(10)$$

with

$$\beta = [1-4\theta_{H_{ads}}(1-\theta_{H_{ads}})(1-\exp(-\omega_{H_{ads}-H_{ads}}/RT))]^{\frac{1}{2}}(11)$$

Note that, the only difference between Eqns. 6 and 9 for one and two-dimensional adsorptions is the expression employed to calculate the configurational entropy term, which in the case of a two-dimensional adsorption is approximated by a Langmuirian configurational expression, while for a one-dimensional adsorption it is exactly derived from statistical thermodynamics for the adsorption of interacting particles [26]. These configurational terms are explicitly subtracted from the adsorbate chemical potential in Eqns. (7) and (10), in order to increase the linearity of $\Delta\overline{G}^{0}_{H_{ads},Global}$vs. $\theta_{H_{ads}}$ at low and high coverages and allow abetter estimation of all deviations from ideality, especially those ones owing to lateral interactions [17,36,46].

When possible changes in the inner layer of H_2O_{ads}, because of H_{ads}/H_2O_{ads} interactions, are explicitly taken into account (Eqn.2), and a negligible coverage of non-occupied platinum sites is considered, the expression for $\theta_{H_{ads}}(E)$ becomes [20,26]:

$$\Delta\overline{G}^{f}_{H_{ads}\&H_2O_{ads},Global} = -FE_{RHE} - RTln(\frac{\theta_{H_{ads}}}{1-\theta_{H_{ads}}}) \text{ on two-dimensional terraces} \quad (12)$$

$$\Delta\overline{G}^{f}_{H_{ads}\&H_2O_{ads},Global} = -FE_{RHE} - RTln(\frac{\beta-1+2\theta_{H_{ads}}}{\beta+1-2\theta_{H_{ads}}}) \text{ on one-dimensional steps} \quad (13)$$

with

$$\Delta\overline{G}^{f}_{H_{ads}\&H_2O_{ads},Global} = \Delta\overline{G}^{0}_{H_{ads},Global} - \Delta\overline{G}^{0}_{H_2O_{ads},Global} - \omega_{H_2O_{ads}-H_2O_{ads}} + \omega_{H_{ads}-H_2O_{ads}} + W_{H_2O_{ads}-H_{ads}}\theta_{H_{ads}}(14)$$

$$\beta = [1-4\theta_{H_{ads}}(1-\theta_{H_{ads}})(1-\exp(-W/RT))]^{\frac{1}{2}}(15)$$

and

$$W_{H_2O_{ads}-H_{ads}} = \omega_{H_{ads}-H_{ads}} + \omega_{H_2O_{ads}-H_2O_{ads}} - 2\omega_{H_{ads}-H_2O_{ads}}(16)$$

in which, $\Delta\overline{G}^{0}_{H_{ads},Global} - \Delta\overline{G}^{0}_{H_2O_{ads},Global}$ is the standard molar Gibbs energy change for Eqn. 2. When comparing Eqns. 12 (13) and 7 (10) a similar mathematical structure is found, with an slightly different physical meaning for equation parameters: in Eqns. 7 (10) $\Delta\overline{G}^{f}_{i,Global}$ and ω_{i-i} corresponds to the formal, coverage-dependent, standard Gibbs energy and the Frumkin-type lateral interaction parameter for adsorption of H_{ads}, while in Eqn. 12 (13) they correspond to the simultaneous adsorption of H_{ads} and the subsequent energetic change in the water adlayer adsorbed on the surface:

$H_2O^{1}_{ads} \rightleftarrows H_2O^{2}_{ads}$(17)

Once hydrogen coverage is measured as a function of the applied potential, the value of $\Delta\overline{G}^{f}_{H_{ads},Global}(\Delta\overline{G}^{f}_{H_{ads}\&H_2O_{ads},Global})$ can be calculated through Eqn.7 (12), or 10 (13). By extrapolation to the zero coverage limit, the standard molar Gibbs energy of adsorption can be also calculated, according to:

$\Delta\overline{G}^{0}_{H_{ads},Global} = \lim_{\theta_{H_{ads}}\to 0} \Delta\overline{G}^{f}_{H_{ads},Global}$(18)

$\Delta\overline{G}^{0}_{H_{ads}\&H_2O_{ads},Global} = \lim_{\theta_{H_{ads}}\to 0} \Delta\overline{G}^{f}_{H_{ads}\&H_2O_{ads},Global} = \Delta\overline{G}^{0}_{H_{ads},Global} - \Delta\overline{G}^{0}_{H_2O_{ads},Global} - \omega_{H_2O_{ads}-H_2O_{ads}} + \omega_{H_{ads}-H_2O_{ads}}$(19)

Additionally, $\omega_{H_{ads}-H_{ads}}$, or $W_{H_2O_{ads}-H_{ads}}$, can be determined from the derivative of $\Delta\overline{G}^{f}_{H_{ads},Global}$ with the coverage:

$\omega_{H_{ads}-H_{ads}} = \left(\frac{\partial\Delta\overline{G}^{f}_{H_{ads},Global}}{\partial\theta_{H_{ads}}}\right)_T$(20)

$W_{H_2O_{ads}-H_{ads}} = \left(\frac{\partial\Delta\overline{G}^{f}_{H_{ads},Global}}{\partial\theta_{H_{ads}}}\right)_T = \omega_{H_{ads}-H_{ads}} + \omega_{H_2O_{ads}-H_2O_{ads}} - 2\omega_{H_{ads}-H_2O_{ads}}$(21)

Figures 2 to 5 summarize the calculated $\Delta\overline{G}^{f}_{i,Global}$ values as function of normalized coverages, at selected temperatures, and of temperature, at fixed coverages, at steps, Figs. 2 and 3, and terraces, Figs. 4 and 5, for Pt(776) and Pt(544), respectively. In the case of steps, $\Delta\overline{G}^{f}_{i,Global}$values were calculated by employing both, one-dimensional and two dimensional expressions: Figs. 2A and 3A vs. 2C and 3C, in order to estimate the inaccuracy that emerges when considering a Langmuirian configurational term to describe the process at step sites, through the mean-field expression, Eqn. 7 (12). Error bars on figures are given only for T = 308.15 K, because they are similar in all data.

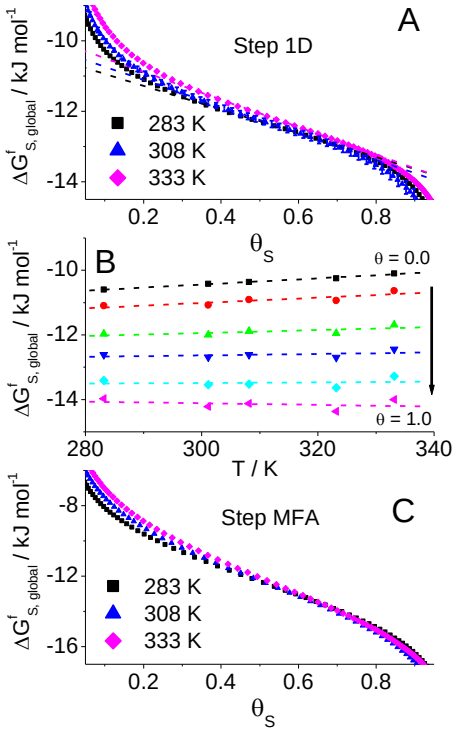

Fig. 2Formal Gibbs energies vs. hydrogen coverage, at selected temperatures for 1D (A) and 2D descriptions (C), and vs. Temperature (B), at selected coverages, at steps, for Pt(776) electrode in 0.1 M $HClO_4$.

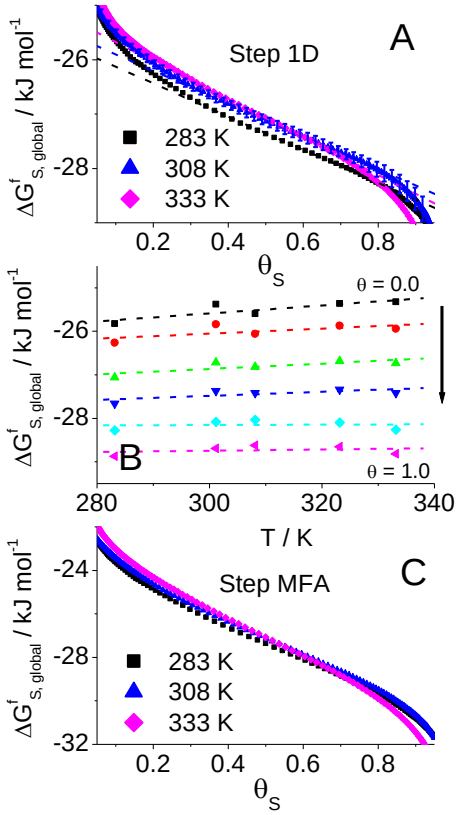

Fig. 3 Formal Gibbs energies vs. hydrogen coverage, at selected temperatures for 1D (A) and 2D descriptions (C), and vs. Temperature (B), at selected coverages, at steps, for Pt(544) electrode in 0.1 M $HClO_4$.

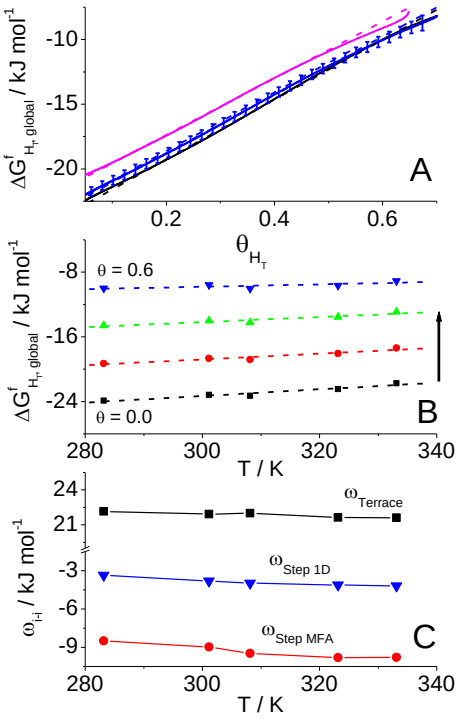

Fig. 4Formal Gibbs energies vs. hydrogen coverage (A), at selected temperatures, vs. Temperature (B), at selected coverages, at terraces, and calculated lateral interaction parameter vs. Temperature (C), for Pt(776) electrode in 0.1 M $HClO_4$.

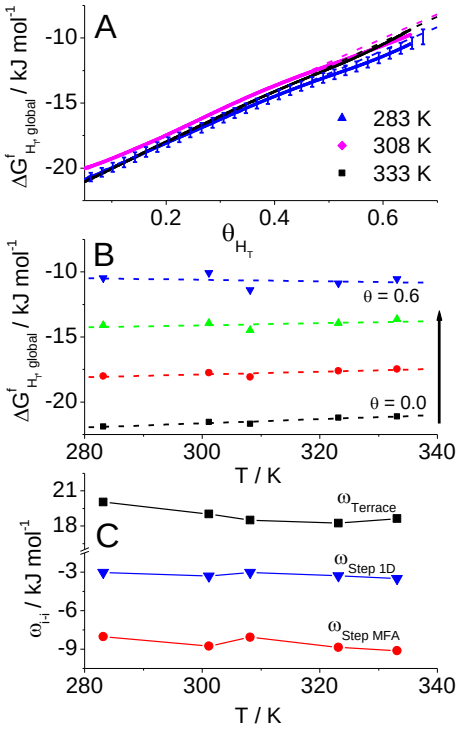

Fig. 5 Formal Gibbs energies vs. hydrogen coverage (A), at selected temperatures, vs. Temperature (B), at selected coverages, at terraces, and calculated lateral interaction parameter vs. Temperature (C), for Pt(544) electrode in 0.1 M $HClO_4$.

In estimating equilibrium coverages of adsorbed species at low potentials and different temperatures, charge densities values, calculated by integration of CVs after subtraction of the double-layer contributions, were normalized by the corresponding surface atomic density expressed in electrical units [11,12,14]. As in previous works, the separation of the voltammetric current in the CV corresponding to the step and terrace contributions was done by assuming that the step site current is simply superimposed to that of the terrace sites [11,12,14]. Thus, these step charges are independent of any hypothesis about the double layer contribution, which is fully included in the terrace charge. In this work, because double-layer capacity values at stepped surfaces are not available, the minimum current measured in the double layer region is chosen as a constant baseline for carrying out double-layer corrections. This is clearly an approximation but, as explained above, good agreement has been found between this and other more precise methods [20,21].

As can be appreciated from Figs. 2A to 5A, formal Gibbs energies at steps are almost coverage-independent, while greater variations are seen at terraces. Nevertheless, for both: steps between $0.2 \leq \theta_{H_{ads}} \leq 0.8$ ML, and terraces between $0.1 \leq \theta_{H_{ads}} \leq 0.55$ ML, $\Delta\overline{G}^{f}_{i,Global}$exhibits a linear dependence on coverage. At low and high coverages, $\Delta\overline{G}^{f}_{i,Global}$deviates from the linear tendency, especially at steps. This could be due to the inability of the model to describe the system at these coverages [47], *i.e.* the real configurational entropy contribution deviates from the configurational entropy term subtracted, Eqns. 7 (12) and 10 (13), or due to the large uncertainty in the determination of $\theta_{H_{ads}}$, which will result in a much large uncertainty in calculated$\Delta\overline{G}^{f}_{i,Global}$ values, because of the logarithmic term in Eqns. 7 (12) and 10 (13). Anyway, linear dynamics at $0.2 \leq \theta_{H_{ads}} \leq 0.8$ ML and $0.1 \leq \theta_{H_{ads}} \leq 0.55$ ML for steps and terraces, respectively, suggest that the adsorption can be described by a Frumkin-type isotherm in this potentials region, as anticipated in Eqns. 7 (12) and 10 (13), and therefore, calculated thermodynamic parameters are extracted from linear fits in this coverage region.

Linear fits of $\Delta\overline{G}^{f}_{i,Global}$ vs. $\theta_{H_{ads}}$ give the standard Gibbs energies of adsorption at different temperatures from intercepts, Figs. 2Bto5B for $\theta_{H_{ads}}$= 0, and the lateral interaction parameters, as a function of temperature, from the slope, Figs. 4Cand 5C. In agreement with that reported for adsorption of H_{ads} on Pt(111), positive values for ω_{i-i} at {111} terraces suggest repulsive interactions between adsorbed particles, while negative ω_{i-i} values at {110} and {100} steps would indicate attractive interactions, as highlighted above. The possible origin of these differences will be discussed below.

Now, taking in to account that:

$$\Delta\overline{G}^{f}_{H_{ads},Global} = \Delta\overline{H}^{f}_{H_{ads},Global} - T\Delta\overline{S}^{f}_{H_{ads},Global} \quad (22)$$

The formal, coverage-dependent, standard entropy change, $\Delta\overline{S}^{f}_{H_{ads},Global}$, can be evaluated from the dependence of $\Delta\overline{G}^{f}_{i,Global}$ on temperature, at constant coverage, Figs. 2B to 5B, as

$$\Delta\overline{S}^{f}_{H_{ads},Global} = -(\frac{\partial\Delta\overline{G}^{f}_{H_{ads},Global}}{\partial T})_{\theta_{H_{ads}}} \quad (23)$$

And then, the formal, coverage-dependent, standard enthalpy change, $\Delta\overline{H}^{f}_{H_{ads},Global}$, can be determined as:

$$\Delta\overline{H}^{f}_{H_{ads},Global} = \Delta\overline{G}^{f}_{H_{ads},Global} + T\Delta\overline{S}^{f}_{H_{ads},Global} \quad (24)$$

In addition, by extrapolating $\Delta\overline{S}^{f}_{H_{ads},Global}$ and $\Delta\overline{H}^{f}_{H_{ads},Global}$ to zero coverage limit, the standard molar entropy and enthalpy of adsorption can be also calculated:

$$\Delta\overline{S}^{0}_{H_{ads},Global} = \lim_{\theta_{H_{ads}}\to 0} \Delta\overline{S}^{f}_{H_{ads},Global} \quad (25)$$

$$\Delta\overline{H}^{0}_{H_{ads},Global} = \lim_{\theta_{H_{ads}}\to 0} \Delta\overline{H}^{f}_{H_{ads},Global} \quad (26)$$

when possible changes in the inner layer of H_2O_{ads}, because of H_{ads}/H_2O_{ads}interactions,are explicitly considered, these Eqns. turn into [20]:

$$\Delta\overline{S}^{0}_{H_{ads}\&H_2O_{ads},Global} = \lim_{\theta_{H_{ads}}\to 0} \Delta\overline{S}^{f}_{H_{ads}\&H_2O_{ads},Global} = \Delta\overline{S}^{0}_{H_{ads},Global} - \Delta\overline{S}^{0}_{H_2O_{ads},Global} - d(\omega_{H_{ads}-H_2O_{ads}} - \omega_{H_2O_{ads}-H_2O_{ads}})/_{dT} \quad (27)$$

$$\Delta\overline{H}^{0}_{H_{ads}\&H_2O_{ads},Global} = \Delta\overline{H}^{0}_{H_{ads},Global} - \Delta\overline{H}^{0}_{H_2O_{ads},Global} - \omega_{H_2O_{ads}-H_2O_{ads}} + \omega_{H_{ads}-H_2O_{ads}} - T\,d(\omega_{H_{ads}-H_2O_{ads}} - \omega_{H_2O_{ads}-H_2O_{ads}})/_{dT} \quad (28)$$

Figures 6 to 9 show formal entropies, $\Delta\overline{S}^{f}_{i,Global}$, and enthalpies, $\Delta\overline{H}^{f}_{i,Global}$, of adsorption at steps, Figs 6 and 7, and terraces, Figs 8 and 9, for Pt(776) and Pt(544), respectively, as a function of hydrogen coverage. For the sake of comparison, $\Delta\overline{S}^{f}_{i,Global}$and $\Delta\overline{H}^{f}_{i,Global}$, values at steps from $\Delta\overline{G}^{f}_{i,Global}$data,calculated by employing two-dimensional expressions, Figs 2C and 3C, are included in Figs. 6 and 7. Error bars for calculated data are also given.

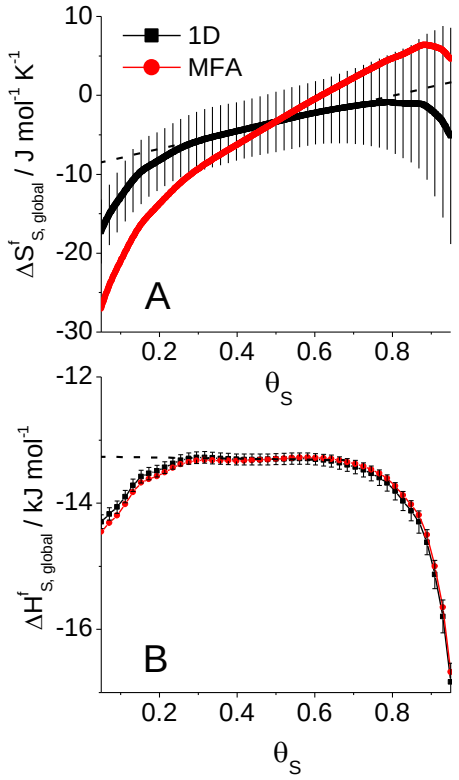

Fig. 6 Formal entropy (A) and enthalpy (B) of adsorption as a function of the coverage at steps, for Pt(776) electrode in 0.1 M $HClO_4$.

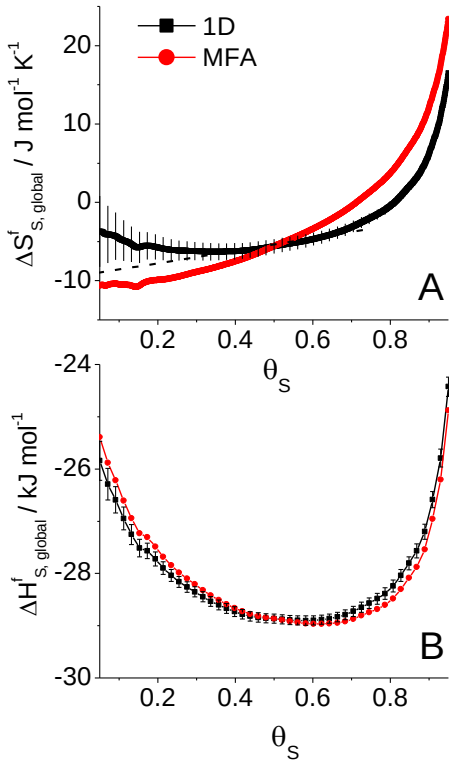

Fig. 7 Formal entropy (A) and enthalpy (B) of adsorption as a function of the coverage at steps, for Pt(544) electrode in 0.1 M $HClO_4$.

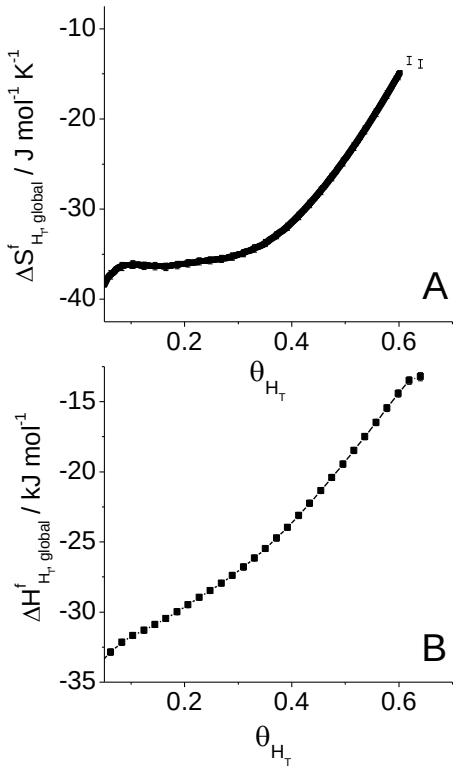

Fig. 8 Formal entropy (A) and enthalpy (B) of adsorption as a function of the coverage at terraces, for Pt(776) electrode in 0.1 M $HClO_4$.

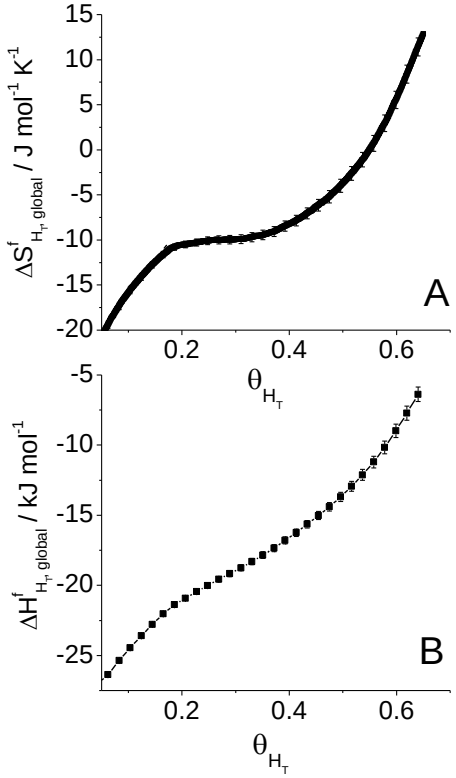

Fig. 9 Formal entropy (A) and enthalpy (B) of adsorption as a function of the coverage at terraces, for Pt(544) electrode in 0.1 M $HClO_4$.

Alternatively, by taking the derivative of Eq. 22 with respect to 1/T, at constant coverage, $\Delta\overline{S}^{f}_{H_{ads},Global}$ and$\Delta\overline{H}^{f}_{H_{ads},Global}$ can be also evaluated:

$$\Delta\overline{H}^{f}_{H_{ads},Global} = \left(\frac{\partial\Delta\overline{G}^{f}_{H_{ads},Global/T}}{\partial T^{-1}}\right)_{\theta_{H_{ads}}} \quad (29)$$

$$\Delta\overline{S}^{f}_{H_{ads},Global} = \frac{\Delta\overline{H}^{f}_{H_{ads},Global} - \Delta\overline{G}^{f}_{H_{ads},Global}}{T} \quad (30)$$

As expected, values of $\Delta\overline{S}^{f}_{H_{ads},Global}$ and $\Delta\overline{H}^{f}_{H_{ads},Global}$ calculated with this second method agree well with those reported in Figs. 6 to9. However, byemploying Eqns. 23 and 24it is possible to estimate the temperature effect on $\Delta\overline{H}^{f}_{H_{ads},Global}$, while Eqns. 29 and 30 allow it for $\Delta\overline{S}^{f}_{H_{ads},Global}$. As anticipated from Fig. 1, all thermodynamic parameters:$\Delta\overline{G}^{f}_{i,Global}$, $\Delta\overline{S}^{f}_{i,Global}$, $\Delta\overline{H}^{f}_{i,Global}$ and ω_{i-i}, areweaker functions of temperature than coverage. The weak dependence of $\Delta\overline{S}^{f}_{i,Global}$ with *T* suggests a low contribution of the vibrational entropy to the total entropy change associated with the adsorption processes [26].

From Figs. 6A to9A, it can be appreciated that entropic changes at steps are weaker functions of the coverage than at terraces, with changes in $\Delta\overline{S}^{f}_{H_{ads}\&H_2O_{ads},Global} \approx 9.8$ and 6.1 J mol^{-1} K^{-1} at steps for Pt(776) and Pt(544), between $0.2 \leq \theta_{H_{ads}} \leq 0.8$ ML, respectively, and ≈ 16.3 J mol^{-1} K^{-1}at terraces for both Pt(776) and Pt(544), with $0.1 \leq \theta_{H_{ads}} \leq 0.55$ ML. In contrast, while $\Delta\overline{S}^{f}_{H_{ads}\&H_2O_{ads},Global}$ at terraces for stepped electrodes are complex functions of coverage,for Pt(111) $\Delta\overline{S}^{f}_{H_{ads}\&H_2O_{ads},Global}$ is a weak, linear function of coverage and the change in $\Delta\overline{S}^{f}_{H_{ads}\&H_2O_{ads},Global}$for H_{ads} is ≈ 10 J mol^{-1} K^{-1}, for $0 \leq \theta_{H_{ads}} \leq 0.6$ ML[20]. A close look into Fig. 8A suggests that for Pt(776) terraces, $\Delta\overline{S}^{f}_{H_{ads}\&H_2O_{ads},Global}$ is a weak, linearfunction of coverage for ≈ $\theta_{H_{ads}} \leq 0.40$ ML, but grows much faster at higher coverages, when $E \leq 0.16$ V and the adsorption at steps begins. Thus, it could be said that H_{ads} adsorption at steps modifies the adlayer ordering at terraces.

For Pt(544), the shape of $\Delta\overline{S}^{f}_{H_{ads}\&H_2O_{ads},Global}$ is more complex, Fig. 9A: it changes fast with $\theta_{H_{ads}}$for$\theta_{H_{ads}} \leq 0.2$ ML, which corresponds to $E < 0.22$ V and the H_{ads} adsorption at steps occurs. For $0.2 \leq \theta_{H_{ads}} \leq 0.4$ ML, and H_{ads} adsorption at steps is completed, it becomes a plateau-like function. Finally, for higher coverages, when $E \leq 0.16$ V, it increases again, even faster than when $\theta_{H_{ads}} \leq 0.2$ ML. Therefore, similar to Pt(776), it looks like adsorption at steps modifies the adlayer order at terraces. In this case, the increase in $\Delta\overline{S}^{f}_{H_{ads}\&H_2O_{ads},Global}$when$E \leq 0.16$ V, is due to adsorption of H_{ads} on the {111} terrace atomic row

adjacent to the step site (the border of the terraces), *i.e.* at the edge of the steps [16]. This adsorption is also given at Pt(s)[(*n*-1)(111)x(110)] surfaces, as can be appreciated inFig. 1. In this case, the adsorption on this site parallels the adsorption at {110} step sites.

Table 1resumes calculated thermodynamic properties of adsorption, at steps and terraces, on Pt(776) and Pt(544) by means of the generalized isotherm, Eqn. 7 (12), and the exact solution of the statistical thermodynamics description for adsorption in one-dimensional steps, Eqn. 10 (13). In this table, the nearest-neighbor interaction energy between two adsorbed molecules is given in parenthesis, andis positive (negative) for repulsive (attractive) interactions. Additionally, temperature averaged $\Delta\overline{G}^{f}_{i,Global}$, $\Delta\overline{S}^{f}_{i,Global}$, $\Delta\overline{H}^{f}_{i,Global}$ and ω_{i-i} values, at low and high coverages for steps, $0.2 \leq \theta_{H_{ads}} \leq 0.8$ ML, and terraces, $0.1 \leq \theta_{H_{ads}} \leq 0.55$ ML, are provided in Table2.As can be appreciated, for both steps, coverage effects on $\Delta\overline{H}^{f}_{i,Global}$ can also be considered negligible, despite attractive effective interactions between adsorbed molecules.

Table 1. Thermodynamic data for the global adsorption processes involved in the low potentials region of cyclic voltammograms of Pt(776) and Pt(533) in 0.1 M $HClO_4$, T = 298.15.*

	$\Delta\overline{G}^{0}_{i,Global}$ / kJ mol^{-1} (eV)	ω_{i-i} / kJ mol^{-1} (eV)	$d\omega_{i-i}/dT$ / J mol^{-1}	$\Delta\overline{S}^{0}_{i,Global}$ / J mol^{-1}	$\Delta\overline{H}^{0}_{i,Global}$ / kJ mol^{-1}
Step on Pt(776) 1D	-10.5 ± 0.2 (-0.11)	-3.7 ± 0.8 (-0.038)	-16.5 ± 2.6	-9.6 ± 2.0	-13.3 ± 0.8
Step on Pt(776) 2D	-7.8 ± 0.8	-9.0 ± 1.5	-28.0 ± 5.0	-17.6 ± 2.6	-13.0 ± 1.6
Step on Pt(544) 1D	-25.6 ± 1.1 (-0.27)	-3.1 ± 1.2 (-0.032)	-7.9 ± 3.9	-9.2 ± 3.5	-28.3 ± 2.1
Step on Pt(544) 2D	-23.0 ± 1.8	-8.3 ± 2.7	-20.0 ± 8.9	-14.5 ± 5.9	-27.3 ± 3.6
Terrace on Pt(776)	-23.4 ± 2.0 (-0.24)	22.0 ± 0.7 (0.038)	-11.7 ± 2.2	-41.1 ± 6.0	-35.7 ± 3.7
Terrace on Pt(544)	-21.7 ± 0.9 (-0.23)	19.3 ± 3.5 (0.033)	-30.5 ± 11.3	-15.9 ± 2.9	-26.4 ± 1.8

*Reported errors reflect the uncertainty associated to $\Delta\overline{G}^{f}_{i,Global}$ and ω_{i-i} vs. *T*least-square regressions.

Table 2.Temperature averaged thermodynamic data for the global adsorption processes involved in the low potentials region of cyclic voltammograms of Pt(776) and Pt(533) in 0.1 M $HClO_4$, at low and high coverages.*

	$\Delta\overline{G}^{f}_{i,Global}$ / kJ mol^{-1}	ω_{i-i} / kJ mol^{-1}	$\Delta\overline{S}^{f}_{i,Global}$ / J mol^{-1}	$\Delta\overline{H}^{f}_{i,Global}$ / kJ mol^{-1}
Step on Pt(776) (1D) θ_i = 0.20 ML	-10.9 ± 0.2	-3.9 ± 0.3	-4.7 ± 0.4	-13.5 ± 0.1
θ_i = 0.80 ML	-13.5 ± 0.1		5.1 ± 0.6	-13.8 ± 0.1
Step on Pt(544) (1D) θ_i = 0.20 ML	-26.0 ± 0.2	-3.2 ± 0.2	-7.6 ± 0.4	-27.8 ± 0.1
θ_i = 0.80 ML	-28.2 ±0.1		-1.55 ± 0.4	-28.3 ± 0.1
Terrace on Pt(776) θ_i = 0.10 ML	-20.5 ± 0.7	21.9 ± 0.3	-35.3 ± 0.7	-31.8 ± 0.2
θ_i = 0.55 ML	-10.6 ± 0.5		-19.1 ± 0.7	-16.8 ± 0.2
Terrace on Pt(544) θ_i = 0.10 ML	-19.7 ± 0.3	18.9 ± 0.7	-15.4 ± 0.5	-24.6 ± 0.2
θ_i = 0.55 ML	-11.5 ± 0.4		1.2 ± 1.3	-11.5 ± 0.4

*Reported errors correspond to standard deviationsoftemperature average values.

When results at steps from the 1D and 2D approximations are compared, it is found that $\Delta\overline{G}^{f}_{i,Global}$ vs. $\theta_{H_{ads}}$plotscalculated by means of the generalized isotherm, Eqn. 7 (12), show a stronger dependence on $\theta_{H_{ads}}$

and more pronounced deviations from linearity, at low and high coverages, than similar curves obtained from the one-dimensional adsorption expression, Figs. 2A and 3A vs. 2C and 3C. These deviations are a direct consequence of the different configurational entropy terms involved in each approximation: $RTln(\frac{\theta_{H_{ads}}}{1-\theta_{H_{ads}}})$ for the 2D adsorption and $RTln(\frac{\beta-1+2\theta_{H_{ads}}}{\beta+1-2\theta_{H_{ads}}})$ for the 1D adsorption. Note that when $\beta = 1$ ($\omega_{i-i} = 0$), the configurational entropy term in both approximations is the same. Additionally, slopes of $\Delta\overline{G}^{f}_{i,Global}$ vs. $\theta_{H_{ads}}$least-square regressions from the 2D equation are steeper, Figs 4C and 5C, and, therefore, higher $\Delta\overline{G}^{0}_{i,Global}$ and lower $\Delta\overline{S}^{0}_{i,Global}$ and ω_{i-i} values are calculated within this approximationat 298.15 K, Table 1. Nevertheless, in both theoretical frameworks similar $\Delta\overline{H}^{f}_{i,Global}$ and $\Delta\overline{H}^{0}_{i,Global}$ values are estimated, Figs 6B and 7B.

Regarding the interaction energy between adsorbed species, $\dot{W}_{H_2O_{ads}-H_{ads}}$, the thermodynamic analysis performed above allows to distinguish between enthalpic, $\omega_{i-i} - Td\omega_{i-i}/dT$, and entropic contributions, $Td\omega_{i-i}/dT$, owing to lateral interactions, Table 3. In this framework, while the enthalpic term is related to changes in the minimum of the potential energy surface (PES), the entropic term deals with variations in the curvature of the PES [21]. As mentioned above, calculated $\dot{W}_{H_2O_{ads}-H_{ads}}$ at steps suggests attractive interactions between adsorbates.However, when enthalpic and entropic contributions are calculated, it is seen that thesenet interactions between species are practically due toentropic contributions. Therefore, it could be said that interactions between adsorbed species arrives because of global changes/reordering of the interface/adsorbed adlayer, and not because of adsorption energy changes of adsorbates, as anticipated from the non-coverage dependence of $\Delta\overline{H}^{f}_{H_{ads}\&H_2O_{ads},Global}$ at steps, Table 2. Contrarily, at terraces, entropic changes are less important and repulsive lateral interactions reflect the decrease in the adsorption energy at increasing coverages.

Table 3. Thermodynamic data for the lateral interactions between adsorbed species at adsorption processes involved in the low potentials region of cyclic voltammograms of Pt(776) and Pt(533) in 0.1 M $HClO_4$, T = 298.15.

	ω_{i-i} / kJ mol^{-1}	$d\omega_{i-i}/dT$ / J mol^{-1}	$Td\omega_{i-i}/dT$ / kJ mol^{-1}	$\omega_{i-i} - Td\omega_{i-i}/dT$ / kJ mol^{-1}
Step on Pt(776) 1D	-3.7 ± 0.8	-16.5 ± 2.6	-4.9 ± 0.8	1.2 ± 1.6
Step on Pt(544) 1D	-3.1 ± 1.2	-7.9 ± 3.9	-2.4 ± 1.2	-0.7 ± 2.4
Terrace on Pt(776)	22.0 ± 0.7	-11.7 ± 2.2	-3.5 ± 0.7	25.5 ± 2.9
Terrace on Pt(544)	19.3 ± 3.5	-30.5 ± 11.3	-9.1 ± 3.4	28.4 ± 6.9

From UHV studies, a repulsive energy of ~28.9 kJ mol^{-1} for H_{ads} on Pt(111) has been reported [48], while on stepped surfaces, a coverage independent binding energy for H_{ads} at steps, *i.e.* $\omega_{H_{ads}-H_{ads}}$ = 0, and a repulsive energy of ~37.8 kJ mol^{-1} at terraces, have been reported [49]. At first sight, a more repulsive $\omega_{H_{ads}-H_{ads}}$ at terraces is contrary to what has been calculated here, becausethe interaction parameter at terraces is less repulsive than that onecalculated for Pt(111), equal to 34.9 kJ mol^{-1} [15,17,20,21]. However, if changes in the inner layer of H_2O_{ads} are explicitly considered, the calculated interaction parameter represents the net effective energetic balance in the adlayer, Eqn. 21, and thus it can be lower than that one at Pt(111), even if $\omega_{H_{ads}-H_{ads}}$ is more repulsive on stepped surfaces. This is because on stepped surfaces $\omega_{H_2O_{ads}-H_2O_{ads}}$ interactions at terraces are less attractive than on Pt(111) as the step density increases [31, 43,50–52], and $\omega_{H_{ads}-H_2O_{ads}}$ are repulsive [31,37,42–44], while on Pt(111) they are attractive [37–41,43,44,53].

Once thermodynamic properties of adsorptionhave been calculated, they will be compared with data fromliterature. Table 4 resumes theoretical free adsorption energies for H_2O, hydrogen, OH and O on different Pt surfaces. Tabulated values correspond to free energies at most stable adsorption sites reported in Refs. [31] and [54]. In these data, solvation and electric field effects in DFT calculations were only includedin Ref. [31] for Pt(111) and Pt(332), using the revised Perdew–Burke–Ernzerhof (RPBE) functional for the exchange–correlation energy. However, calculated $\Delta\overline{G}^0_{H_2O_{ads}}$ for {110} and {100} stepped surfaces are quite similar and thus, changes in $\Delta\overline{G}^0_{i_{ads}}$because of solvation and the electric double layer from Ref. [31] can be used, as first approximation, to "correct" the$\Delta\overline{G}^0_{i_{ads}}$ vacuum data calculated in Ref. [54]. Additionally, because PBE gives a better result for H_{ads} than RPBE, while RPBE gives a better result for O_{ads} than PBE [31],$\Delta\overline{G}^0_{i_{ads}}$ on electrically neutral surfaces in vacuum, calculated using the PBE functional in Ref [31], were also "adjusted" and reportedinTable 4.

Because the water adlayer is considered in Table 4, tabulated values are good approximations for $\Delta\overline{G}^0_{H_{ads}\&H_2O_{ads},Global}$, Eqn. 19. When comparing $\Delta\overline{G}^0_{H_{ads}}$values in Table 4 with $\Delta\overline{G}^0_{H_{ads}\&H_2O_{ads},Global}$values in Table 1 a good agreement is found if the comparison is done with$\Delta\overline{G}^0_{H_{ads}}$values at steps that include solvation and electric double layer effects, but higher differences are found for the adsorption at terraces. Note that, according to data in Table 4, the adsorption of hydroxyl from water dissociation in principle could happen at steps (on Pt(533), $\Delta\overline{G}^0_{HO_{ads}}$ = 0.11 eV). However, this value was estimated from calculations for {110} stepped surfaces, for which a stabilization of OH_{ads} at steps from the OH/water network at terraces is

anticipated. Contrarily, for {100} stepped surfaces, a destabilization of OH_{ads} at steps, because of OH/water network at terraces, is expected [32]. Therefore, approximated $\Delta\overline{G}^{0}_{HO_{ads}}$ for Pt(533) to include solvation and electric field effects in Table 4 is underestimated.

Table 4. Free adsorption energies for H_2O, hydrogen, OH and O on different Pt surfaces (most stable adsorption sites)

	$\Delta\overline{G}^{0}_{H_2O_{ads}}$ / eV	$\Delta\overline{G}^{0}_{H_{ads}}$ / eV	$\Delta\overline{G}^{0}_{HO_{ads}}$ / eV	$\Delta\overline{G}^{0}_{O_{ads}}$ / eV
Pt(111) [a]	0.28	-0.29/-0.29	1.02/0.48	1.23/1.27
Pt(111) [b]	0.28/0.18*	-0.13/-0.30	0.69/0.61	0.84/0.79
Pt(332) Step [b]	0.07/0.04*	0.04/-0.12	0.76/0.45	0.94/0.91
Terrace	0.19/0.00*	-0.10/-0.25	0.82/0.69	0.96/0.89
Pt(553) Step [a]	0.07	-0.28/-0.16	0.66/0.50	1.45/1.56
Terrace	0.24	-0.21/-0.18	1.16/0.75	1.08/1.08
Pt(533) Step [a]	0.06	-0.41/-0.29	0.27/0.11	1.41/1.52
Terrace	0.27	-0.21/-0.18	1.08/0.67	0.94/1.18

[a] First and second values correspond to theoretical data from Ref. [54] and valuescalculated from these data butincluding solvation and electric field effects reported in Ref. [31], respectively.

[b] First and second values correspond to RPBE results in Ref [31], and estimated values from PBE free adsorption energies on electrically neutral surfaces in vacuum and including solvation and electric field effects calculated in the same work, respectively. * Estimated values from adsorption energies per H_2O for interfacial water. First and second values correspond to adsorption energies of isolated molecules and most stable water bilayers, respectively.

From the entropy of the global reaction, Eqn. 27, and the tabulated value of the entropy change to the reaction on the RHE reference electrode, $\Delta\overline{S}^{0}_{RHE}$ = 61.75 J mol^{-1} K^{-1} [20,21], the entropy of the adsorptionprocess can be calculated from [20,21]:

$$\Delta\overline{S}^{0}_{H_{ads}\&H_2O_{ads}} = \Delta\overline{S}^{0}_{H_{ads}\&H_2O_{ads},Global} + \Delta\overline{S}^{0}_{RHE} \quad (31)$$

Table 5summarizes $\Delta\overline{S}^{0}_{H_{ads}\&H_2O_{ads}}$ values for Pt(776) and Pt(544) at steps and terraces.From these values and a model based on simple statistical thermodynamic considerations, the entropy of the adsorbed species as a function of the coverage can be compared with the entropy of a fully mobile or immobile adlayer, in order to gain some knowledge about the mobility of the adsorbed species. For Pt(111), $\Delta\overline{S}^{0}_{H_{ads},immobile}$ and $\Delta\overline{S}^{0}_{H_{ads},mobile}$ values are 5.3 and 32.3 J mol^{-1} K^{-1}, respectively [20], and they are similar to $\Delta\overline{S}^{0}_{H_{ads},immobile}$ and $\Delta\overline{S}^{0}_{H_{ads},mobile}$ values for Pt(100)and Pt(110) surfaces [20]. Therefore, because $\Delta\overline{S}^{0}_{H_{ads}\&H_2O_{ads}}$ in Table 5 liesbetween20.6 to 52.6 J mol^{-1} K^{-1}, it could be assumed that in all cases adsorbed hydrogen has a high surface

diffusion. However, calculated $\Delta\overline{S}^{0}_{H_{ads}\&H_2O_{ads}}$is a global parameter that includes $\Delta\overline{S}^{0}_{H_{ads}}$, $\Delta\overline{S}^{0}_{H_2O_{ads}}$ and $d(\omega_{H_{ads}-H_2O_{ads}} - \omega_{H_2O_{ads}-H_2O_{ads}})/_{dT}$ terms, Eqn. 27. Therefore, if H_{ads} destabilizes the adsorbed water adlayer, as on stepped surfaces [31,37,42,43,44], lower $\Delta\overline{S}^{0}_{H_{ads}}$values than those reported in Table 5 are expected. Contrarily, if H_{ads}stabilizeswater adsorption, as on Pt(111) [37–41,43,44,53], higher $\Delta\overline{S}^{0}_{H_{ads}}$values are anticipated.

Table 5.$\Delta\overline{S}^{0}_{H_{ads}\&H_2O_{ads}}$, $\Delta\overline{H}^{0}_{H_{ads}\&H_2O_{ads}}$and $E_{Pt-H}$for the adsorption processes involved in the low potentials region of cyclic voltammograms of Pt(776) and Pt(533) in 0.1 M $HClO_4$, T = 298.15.*

	$\Delta\overline{S}^{0}_{H_{ads}\&H_2O_{ads}}$ / J mol^{-1}	$\Delta\overline{H}^{0}_{H_{ads}\&H_2O_{ads}}$ / kJ mol^{-1}	E_{Pt-H} / kJ mol^{-1}
Step on Pt(776) 1D	52.2 ± 2.0	5.1 ± 0.8	231.3
Step on Pt(544) 1D	52.6 ± 3.5	-9.9 ± 2.1	246.3
Terrace on Pt(776)	20.6 ± 6.0	-17.3 ± 3.7	253.7
Terrace on Pt(544)	45.8 ± 2.9	-8.0 ± 1.8	244.4

Finally, $\Delta\overline{H}^{0}_{H_{ads}\&H_2O_{ads},Global}$values in Table 1 can be employed to estimate the energy of the Pt-H bond and the enthalpy of the adsorbed process,$\Delta\overline{H}^{0}_{H_{ads}\&H_2O_{ads}}$. However, similarly to $\Delta\overline{S}^{0}_{H_{ads}\&H_2O_{ads}}$, calculated values will represent global parameters, including $\Delta\overline{H}^{0}_{H_{ads}}$, $\Delta\overline{H}^{0}_{H_2O_{ads}}$, $\omega_{H_2O_{ads}-H_2O_{ads}}$, $\omega_{H_{ads}-H_2O_{ads}}$and $T\,d(\omega_{H_{ads}-H_2O_{ads}} - \omega_{H_2O_{ads}-H_2O_{ads}})/_{dT}$ terms, Eqn. 28,[21]:

$$\Delta\overline{H}^{0}_{H_{ads}\&H_2O_{ads}} = \Delta\overline{H}^{0}_{H_{ads}\&H_2O_{ads},Global} + T\Delta\overline{S}^{0}_{RHE} \quad (32)$$

$$E_{Pt-H} = 1/2D_{H_2} - \Delta\overline{H}^{0}_{H_{ads}\&H_2O_{ads},Global} \quad (33)$$

WhereD_{H_2}= 435.99 kJ mol^{-1} is the enthalpy of dissociation of H_2 [21]. Calculated values for $\Delta\overline{H}^{0}_{H_{ads}\&H_2O_{ads}}$ and E_{Pt-H} are given in Table 5. As can be seen, apparently, E_{Pt-H} bonds are stronger at terraces than steps on Pt(776) while it is slightly higher at steps than at terraces on Pt(544). In contrast, in UHV environment, higher differences between E_{Pt-H} bonds at steps and terraces are reported, ranging from 311 to 263 kJ mol^{-1} at {110} steps [49,52], 299 to 261 kJ mol^{-1} at {100} steps [52,55], and 281 to 293 kJ mol^{-1} at {111} terraces[49,52].Nevertheless, if changes in the adsorption enthalpy because of water environment are considered, tabulated values at steps and terraces should increase ~15 and 3 kJ mol^{-1} [31]. On the other hand, the fact that the enthalpy change associated to hydrogen adsorption is positive at {110} steps strongly supports the idea that this enthalpy change is not only influenced by the chemical interaction between adsorbed hydrogen and the platinum surface. Here it is important to highlight that any double-layer

contribution to values in Table 5 has been neglected, although this term only would modify calculated values for terraces, as mentioned above.

3.2 Changes in the standard molar Gibbs energy with the step density at low potentials.

In order to evaluate the effect of the step density in $\Delta\overline{G}^{0}_{H_{ads}\&H_2O_{ads},Global}$ and $\dot{W}_{H_2O_{ads}-H_{ads}}$ at step and terraces, $\Delta\overline{G}^{f}_{i,Global}$ values as function of normalized coverages, at room temperature, $T \approx 301.15$ K, were calculated from cyclic voltammograms for different Pt(s)[(*n*-1)(111)x(110)], $n \geq 5$, and Pt(S)[*n*(111)x(100)], $n \geq 4$, stepped surfaces, following the same procedure explained above. Also, $\Delta\overline{G}^{0}_{H_{ads}\&H_2O_{ads},Global}$ and $\dot{W}_{H_2O_{ads}-H_{ads}}$ values are calculated from intercepts and slopes of linear $\Delta\overline{G}^{0}_{H_{ads}\&H_2O_{ads},Global}$ vs. $\theta_{H_{ads}}$ least-square regressions. For adsorption process at steps, $\Delta\overline{G}^{f}_{i,Global}$ values were calculated by employing the one-dimensional expression, Eqn. 10 (13). Calculated $\Delta\overline{G}^{0}_{H_{ads}\&H_2O_{ads},Global}$ and $\dot{W}_{H_2O_{ads}-H_{ads}}$ values at step and terraces are given in Figures 10 and 11, respectively.

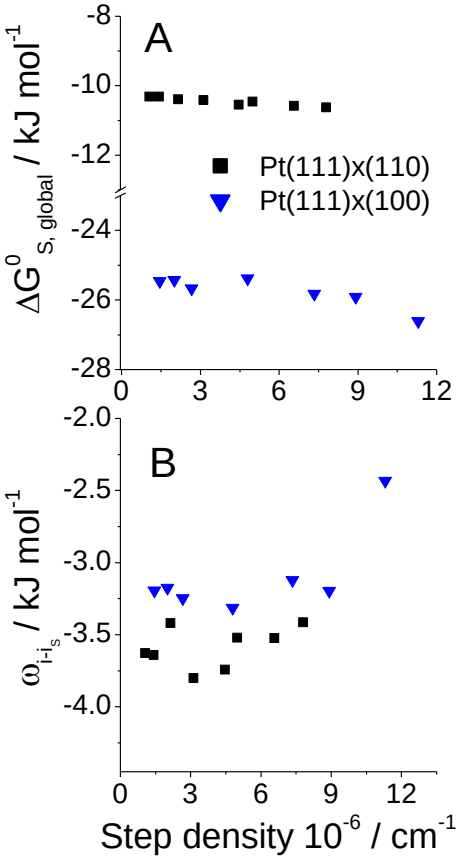

Fig. 10 Standard molar Gibbs energy of adsorption (A) and effective lateral interaction parameter (B) associated to step sites, as a function of step density in 0.1 M $HClO_4$, at room temperatures, for Pt(s)[(*n*-1)(111)x(110)] and Pt(S)[*n*(111)x(100)], as indicated.

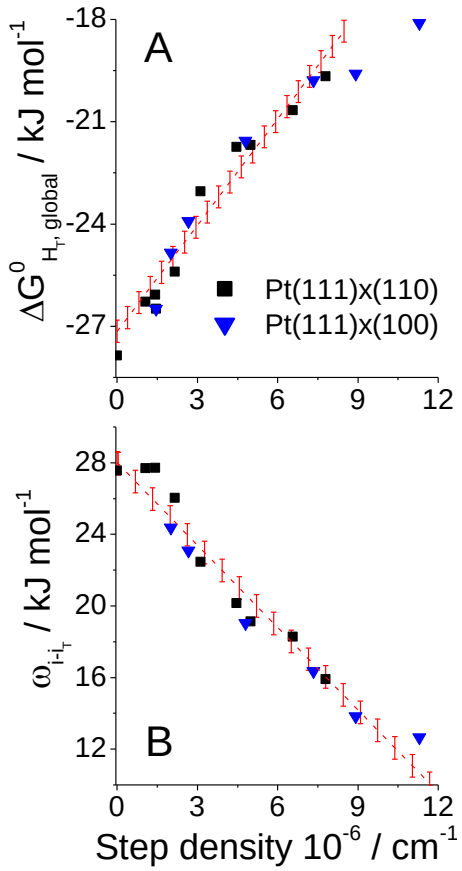

Fig. 11 Standard molar Gibbs energy of adsorption (A) and effective lateral interaction parameter (B) associated to terrace sites, as a function of step density in 0.1 M $HClO_4$, at room temperatures, for Pt(s)[(*n*-1)(111)x(110)] and Pt(S)[*n*(111)x(100)], as indicated.

As expected from the non-dependence of peak potentials on the step density, results from Fig. 10 show that $\Delta\overline{G}^{0}_{H_{ads}\&H_2O_{ads},Global}$ ($W_{H_2O_{ads}-H_{ads}}$) values are practically independent of the step density, for $n \geq 5$, with average values of≈ -10.5 ± 0.1 (-3.6 ± 0.1) and -25.6 ± 0.2 (-3.2 ± 0.1) kJ mol^{-1} for Pt(s)[(*n*-1)(111)x(110)] and Pt(S)[*n*(111)x(100)], respectively. At Pt(533), $n = 4$, $\Delta\overline{G}^{0}_{H_{ads}\&H_2O_{ads},Global}$ ($W_{H_2O_{ads}-H_{ads}}$) is -26.6 (-2.4) kJ mol^{-1}, slightly lower (higher) than average values for the Pt(S)[*n*(111)x(100)] series. This could be because at this short terrace width individual steps are close enough, no longer isolated from each other and an interaction between neighbor step dipoles may occur [14].In agreement, the peak shape at low potentials becomes slightly wider. At even higher step densities, this peak splits as it appears in the limiting cases of Pt(311) and Pt(110) in perchloric acid solutions for flame annealed surfaces cold in hydrogen [14].

In contrast, results from Fig. 11 illustrate that $\Delta\overline{G}^{0}_{H_{ads}\&H_2O_{ads},Global}$ ($W_{H_2O_{ads}-H_{ads}}$) increases (decreases) with increasing step density, following a linear tendency for $n \geq 5$, with an intercept equal to -26.9 (28.0) kJ mol^{-1}, close to $\Delta\overline{G}^{0}_{H_{ads}\&H_2O_{ads},Global}$ ($W_{H_2O_{ads}-H_{ads}}$) value calculated for the Pt(111) surface, -27.9 (29.2) kJ mol^{-}

[1][20]. Slopes from least-square regressions for $\Delta\overline{G}^{0}_{H_{ads}\&H_2O_{ads},Global}$ and $\dot{W}_{H_2O_{ads}-H_{ads}}$ in Fig. 11 are 0.95 and 1.5 (absolute values), suggesting a stronger influence of step in the net energetic balance between adsorbed species than in adsorbed energies. This can be interpreted in term of a dominant role of $\omega_{H_{ads}-H_2O_{ads}}$ interactions in the adlayer balance. At lower *n* values, the $\Delta\overline{G}^{0}_{H_{ads}\&H_2O_{ads},Global}$ ($\dot{W}_{H_2O_{ads}-H_{ads}}$) value increases (decreases) less than expected form the linear tendency and this could be due to interactions between neighbor step dipoles, as suggested above.

One important fact, derived from Fig 11, is the problem to solely ascribe the adsorption process at terraces as hydrogen adsorption, as in Eqn. 3, in which case a less repulsive interaction parameter, $\omega_{i_{ads}-i_{ads}}$ should decrease $\Delta\overline{G}^{f}_{H_{ads},Global}$, Eqn. 8. Contrarily, Fig. 11 evidences an increase in $\Delta\overline{G}^{0}_{H_{ads},Global}$ as the step density increases, despite the lower interaction parameter. Additionally, a similar effect of both {110} and {100} steps on the H_{ads} adsorption dynamics at terraces strongly suggests a common origin. However, adsorption of H_{ads} at terraces on {111} vicinal surfaces with {110} and {100} steps takes place under to two different H_{ads}-coverages at steps: while on [*n-1*(111)x(110)] surfaces most of the H_{ads} adsorption at terrace occurs under a H_{ads}-free {110} step, on [*n*(111)x(100)] surfaces the adsorption of H_{ads} at terraces and steps simultaneously begins and, once the step is saturated, additional H_{ads} adsorption at terraces occurs with a H_{ads}-saturated step. Therefore, it is more probable that changes in the stable H_2O_{ads} network, and not because of H_{ads} at steps, are responsible of the energetic changes at terraces at increasing step densities.

Additional evidence about the role of the adsorbed water adlayer in the hydrogen adsorption dynamics in electrochemical environments is suggested by noting that changes in $\Delta\overline{G}^{0}_{H_{ads}\&H_2O_{ads},Global}$, in Fig. 11, follow the changes in the potential of maximum entropy (pme) at terraces at increasing step densities [18]. In this sense, the increase in the pme at terraces with high step densities increases the electric field at potentials where H_{ads} occurs, which in turn would decrease the $\omega_{H_{ads}-H_2O_{ads}}$ attractive interactions. This is because at increasing negative potentials, water molecules would prefer the O-up configuration and the distance between the interacting oxygen and adsorbed hydrogen atoms would increase, weakening their mutual interaction [53]. In this case, considering Eqn. 19 (21), a higher (lower) $\Delta\overline{G}^{0}_{H_{ads}\&H_2O_{ads},Global}$ ($\dot{W}_{H_2O_{ads}-H_{ads}}$) value is calculated.

Evidence of H-bonding between H_{ads} and H_2O_{ads} has also been suggested from surface spectroscopy studies [1,2]. Inside this framework, the lower $\Delta\overline{G}^{0}_{H_{ads}\&H_2O_{ads},Global}$ value reported for Pt(111) in alkaline

electrolytes, ≈ 22 kJ mol^{-1} [15], could be originated because of a higher pme in this electrolyte than in acid media. Indeed, considering results in Fig. 11 and Fig. 8B in Ref. [18], in which the change in the pme associated at terraces with the step density in 0.1 M $HClO_4$ is reported, a pme around ~0.57 V in alkaline solutions is estimated, taking into account the 0.12 V shift in the peak potentials at steps in alkaline electrolytes compared to perchloric solutions.

3.3 Adsorption of OH_{ads}, or O_{ads}, on step sites at low potentials.

Let´s now discuss the possibility that the adsorption process taking place at low potentials at steps is not because of water and H_{ads} co-adsorption, but it may involve the formation of OH_{ads}, or O_{ads}. In the case of H_{ads} and OH_{ads}co-adsorption, Eqn. 1 becomes

$$H_{ads} + H_2O \rightleftarrows OH_{ads} + H_2 \quad (34)$$

and the Eqn. 12 for the one-dimensional adsorption, and assuming a negligible coverage of non-occupied platinum sites, would be given by

$$\Delta\overline{G}^{f}_{H_{ads}\&OH_{ads},Global} = -2FE_{RHE} - RTln(\frac{\beta-1+2\theta_{H_{ads}}}{\beta+1-2\theta_{H_{ads}}}) \quad (35)$$

with

$$\Delta\overline{G}^{f}_{H_{ads}\&OH_{ads},Global} = \Delta\overline{G}^{0}_{H_{ads},Global} - \Delta\overline{G}^{0}_{OH_{ads},Global} - \omega_{OH_{ads}-OH_{ads}} + \omega_{H_{ads}-OH_{ads}} + \dot{W}_{HO_{ads}-H_{ads}}\theta_{H_{ads}}$$

$$\dot{W}_{OH_{ads}-H_{ads}} = \omega_{H_{ads}-H_{ads}} + \omega_{OH_{ads}-OH_{ads}} - 2\omega_{H_{ads}-OH_{ads}} \quad (36)$$

As can be seen, the only difference between Eqns. 12 and 35 is the number of electrons transferred in the reaction, one and two, respectively. In the same way, if H_{ads} and O_{ads} co-adsorption is considered, Eqn. 1 turns into

$$H_{ads} + H_2O \rightleftarrows xO_{ads} + 3/2H_2 \quad (37)$$

and the equation for the one-dimensional adsorption will be as Eqn. 35 but involving a 3-electron transfer. In order to estimate the change in the calculated values given in the previous section, when applying Eqn. 35 instead of Eqn. 12, $\Delta\overline{G}^{f}_{i,Global}$, $\Delta\overline{S}^{f}_{i,Global}$ and $\Delta\overline{H}^{f}_{i,Global}$values were calculated for Pt(776) and Pt(544), but employing Eqns. 35 and 36.Figures 12 and 13 depicts $\Delta\overline{G}^{f}_{i,Global}$ at $T \approx 301.15$ K, $\Delta\overline{S}^{f}_{i,Global}$ and $\Delta\overline{H}^{f}_{i,Global}$ values as functions of normalized coverages, for adsorption processes at steps on Pt(776) and Pt(544), respectively, when the adsorption process at steps is considered to follow Eqn. 34. For the sake of comparison, $\Delta\overline{G}^{f}_{i,Global}$, $\Delta\overline{S}^{f}_{i,Global}$ and $\Delta\overline{H}^{f}_{i,Global}$ values in Figs. 12 and 13 are given divided by two, and calculated $\Delta\overline{G}^{f}_{i,Global}$, $\Delta\overline{S}^{f}_{i,Global}$ and $\Delta\overline{H}^{f}_{i,Global}$ values found in the previous section, when the transference of

one electron was assumed, are also given.

As can be appreciated from Figs. 12 and 13, if the adsorption states at low potentials are due to H_{ads} and OH_{ads}, instead of H_{ads} and H_2O_{ads}, similar tendencies are obtained, and $\Delta\overline{G}^{f}_{i,Global}$, $\Delta\overline{S}^{f}_{i,Global}$ and $\Delta\overline{H}^{f}_{i,Global}$ values would be similar to those reported in Tables 1 and 2, but multiplied by the number of electrons transferred in the reaction, *i.e.*, 2. Nevertheless, because the slope in the $\Delta\overline{G}^{f}_{i,Global}$ vs. $\theta_{H_{ads}}$ curves becomes less steep, smaller attractive lateral interactions would result than in the case of H_{ads} and H_2O_{ads} co-adsorption.

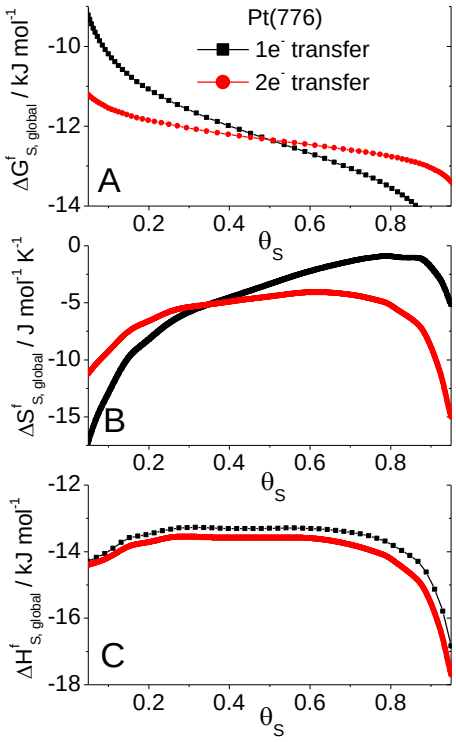

Fig. 12 Formal Gibbs energies (A), entropy (B), and enthalpy (C), for H_{ads} and H_2O_{ads} ($1e^-$ transfer), and H_{ads} and OH_{ads} ($2e^-$ transfer) co-adsorption vs. hydrogen coverage at steps on Pt(776) in 0.1 M $HClO_4$.

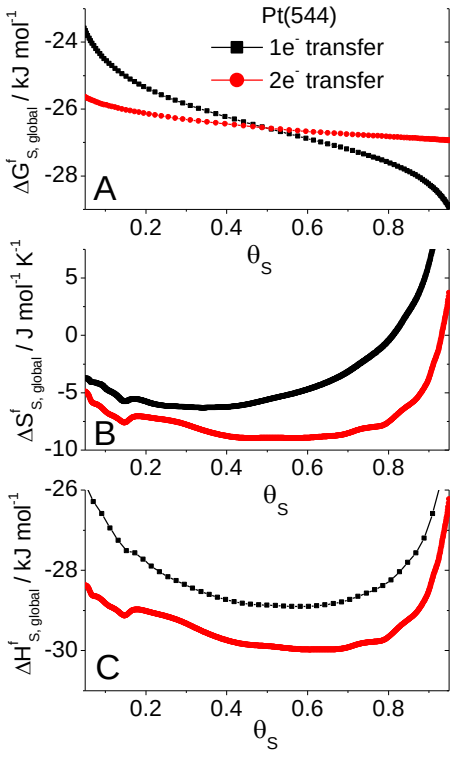

Fig. 13 Formal Gibbs energies (A), entropy (B), and enthalpy (C), for H_{ads} and H_2O_{ads} ($1e^-$ transfer), and H_{ads} and OH_{ads} ($2e^-$ transfer) co-adsorption vs. hydrogen coverage at steps on Pt(544) in 0.1 M $HClO_4$.

On the other hand, from a physical point of view, reaction schemes involving more than one transferred electron would imply $\theta_{H_{ads}} \leq 1.0$ ML at the steps at saturation, and the decrease in $\theta_{H_{ads}}$ should be proportional to the coverage at saturation of the co-adsorbed species and the number of transferred electrons. Qualitatively, the possible existence of OH_{ads}, or O_{ads}, at low potentials at steps of stepped surfaces can be assessed by calculating expected reversible potentials for reactions34 and 37. In this sense, theoretical values in Table 4 are employed and the estimated reversible potentials are reported in Table 6. For the sake of completeness, the reversible potential for co-adsorption of H_{ads}, OH_{ads} and O_{ads}, through reaction 38, is also given.

$$H_{ads} + 2H_2O \rightleftarrows O_{ads} + OH_{ads} + 2H_2 \quad (38)$$

Table 6. Estimated reversible potentials for reactions 2, 34, 37 and 38on different Pt surfaces

	$J^0_{H_{ads}\&H_2O_{ads}}$ / eV	$U^0_{H_{ads}\&OH_{ads}}$ / eV	$U^0_{H_{ads}\&O_{ads}}$ / eV	$U^0_{H_{ads}\&OH_{ads}\&O_{ads}}$ / eV
Pt(111) [a]	0.29	0.66/0.39	0.51/0.52	0.64/0.51
Pt(111) [b]	0.13/0.30	0.41/0.46	0.32/0.36	0.42/0.43
Pt(332) Step [b]	-0.04/0.12	0.36/0.29	0.27/0.30	0.39/0.34
Terrace	0.10/0.25	0.46/0.47	0.35/0.38	0.47/0.46
Pt(553) Step [a]	0.28/0.16	0.47/0.26	0.45/0.41	0.51/0.40
Terrace	0.21/0.18	0.69/0.47	0.55/0.58	0.71/0.62
Pt(533) Step [a]	0.41/0.29	0.34/0.33	0.54/0.53	0.41/0.43
Terrace	0.21/0.18	0.65/0.43	0.45/0.57	0.68/0.59

[a] First and second values were calculated from theoretical data from Ref. [54] and including solvation and electric field effects reported in Ref. [31] to these latter values, as in Table 4, respectively.

[b] First and second values were calculated from RPBE and PBE theoretical data from Ref. [31] in Table 4, respectively.

From the reversible potential values given in Table 6 it can be seen that co-adsorption of H_{ads} and H_2O_{ads} is the most probable process to take place at steps in acidic electrolytes, because for this process $U^0_{H_{ads}\&H_2O_{ads}}$ values are reasonably in agreement with data in Table 1.It could be said that, when calculating reversible potentials in Table 6, interactions between species for $U^0_{H_{ads}\&OH_{ads}}$, $U^0_{H_{ads}\&O_{ads}}$ and $U^0_{H_{ads}\&OH_{ads}\&O_{ads}}$ are not included and so, calculated potentials could be overestimated. In order to estimate the effect of lateral interactions between adsorbates in $U^0_{H_{ads}\&i_{ads}}$, some previous considerations should be done. From Eqn. 21, the $\omega_{H_{ads}-i_{ads}}$ interaction can be expressed as function of the global interaction parameter calculated from experiments, $\dot{W}_{i_{ads}-H_{ads}}$, as

$$\omega_{H_{ads}-i_{ads}} = (\omega_{H_{ads}-H_{ads}} + \omega_{i_{ads}-i_{ads}} - \dot{W}_{i_{ads}-H_{ads}})/2 \quad (39)$$

by employing this equation to estimate the difference between $\omega_{H_{ads}-i_{ads}}$ and $\omega_{i_{ads}-i_{ads}}$ in Eqn. 19

$$\omega_{H_{ads}-i_{ads}} - \omega_{i_{ads}-i_{ads}} = (\omega_{H_{ads}-H_{ads}} - \omega_{i_{ads}-i_{ads}} - \dot{W}_{i_{ads}-H_{ads}})/2 \quad (40)$$

and considering $\omega_{H_{ads}-H_{ads}}$= 0, as reported from UHV studies [49], Eqn. 40 can be rewritten as

$$\omega_{H_{ads}-i_{ads}} - \omega_{i_{ads}-i_{ads}} = (-\omega_{i_{ads}-i_{ads}} - \dot{W}_{i_{ads}-H_{ads}})/2 \quad (41)$$

Now, because $\dot{W}_{i_{ads}-H_{ads}}$ is attractive, as well as usually $\omega_{OH_{ads}-OH_{ads}}$ does, a decrease in $U^0_{H_{ads}\&OH_{ads}}$ is expected. Taking $\omega_{OH_{ads}-OH_{ads}} \approx$ -0.20 eV, the highest calculated value for OH_{ad}-OH_{ads} interactions at Pt(111) [56], and $\dot{W}_{i_{ads}-H_{ads}}$ = -0.038 eV, as in Table 1, the maximum decrease expected in $U^0_{H_{ads}\&OH_{ads}}$would be~0.06 eV. Contrarily, because usually $\omega_{O_{ads}-O_{ads}}$ are repulsive, the maximum anticipated decrease in $U^0_{H_{ads}\&O_{ads}}$would be ~0.01 eV. For $U^0_{H_{ads}\&OH_{ads}\&O_{ads}}$, an intermediate value between these two cases would be expected. In consequence, even including the effect of lateral interactions in $U^0_{H_{ads}\&i_{ads}}$, the co-adsorption of H_{ads} and H_2O_{ads} is the most probable process to occur at {110} steps in acidic electrolytes. It would be the same in {100} steps, because of the similarity between adsorption processes at {110} and {100} steps. Here, it should be emphasized that in Table 6 calculated potentials involving OH_{ads} free energy at {100} steps are underestimated, as explained above. However, in alkaline electrolytes, because the adsorption process at steps shifts to higher potentials, co-adsorption of OH_{ads} could actually occur.

5. Conclusions

In the present work a thermodynamic analysis of adsorption processes in the voltammetric profile of {111} vicinal platinum surfaces at low potentials is performed and thermodynamic properties such as the formal entropies, $\Delta\overline{S}^{f}_{i,Global}$, enthalpies, $\Delta\overline{H}^{f}_{i,Global}$, and Gibbs energies, $\Delta\overline{G}^{f}_{i,Global}$, of adsorption processes at two-dimensional terraces and one-dimensional steps are calculated. Results are interpreted in terms of the interaction between adsorbed hydrogen, H_{ads}, and the water network, H_2O_{ads}, already adsorbed on the electrode. Calculated values show that all thermodynamic parameters:$\Delta\overline{G}^{f}_{i,Global}$, $\Delta\overline{S}^{f}_{i,Global}$ and $\Delta\overline{H}^{f}_{i,Global}$ are weaker functions of temperature than coverage. In addition,formal Gibbs energies and entropies at steps are almost coverage-independent, while greater variations are estimatedat terraces.

When the effect of the step density on the standard Gibbs energy and on the lateral interactions between adsorbed species at terraces and steps is determined, it is found that that $\Delta\overline{G}^{0}_{H_{ads}\&H_2O_{ads},Global}$ ($W_{H_2O_{ads}-H_{ads}}$) values at steps are practically independent of the step density, but, as expected, $\Delta\overline{G}^{0}_{H_{ads}\&H_2O_{ads},Global}$ values depend on the step orientation. In contrast, $\Delta\overline{G}^{0}_{H_{ads}\&H_2O_{ads},Global}(W_{H_2O_{ads}-H_{ads}})$ at terraces increases (decreases) with the step density, following an almost linear tendency for *n*> 5. Results highlight the role of the adsorbed water adlayer in the hydrogen adsorption dynamics in electrochemical environments and the importance of$\omega_{H_{ads}-H_2O_{ads}}$interactions in the adlayer energetic balance.

Comparing experimental results with theoretical data from literature suggest that the co-adsorption of H_{ads} and H_2O_{ads} is the most probable process to occur at {110} steps in acidic electrolytes, and also at {100} steps, because of the similarity between adsorption processes at {110} and {100} steps. However, as the adsorption processes at steps in alkaline electrolytes shift to higher potentials, co-adsorption of OH_{ads} could occur in this latter solution and specific data are required to evaluate this possibility.

Acknowledgments

This study has been carried out in the framework of the European Commission FP7 Initial Training Network ‘‘ELCAT’’, Grant Agreement No. 214936–2.Support from the Spanish MINECO though project CTQ2013–44083-P and GV through PROMETEOII/2014/013 (FEDER) are greatly acknowledged.

References

1. B.E. Conway, B.V. Tilak, Interfacial processes involving electrocatalytic evolution and oxidation of H_2, and the role of chemisorbed H, Electrochim. Acta 47 (2002) 3571-3594.
2. R.J. Nichols, A. Bewick, Spectroscopic identification of the adsorbed intermediate in hydrogen evolution on platinum, J. Electroanal. Chem. 243 (1988) 445-453.

3. D. Strmcnik, D. Tripkovic, D. van der Vliet, V. Stamenkovic, N.M. Markovic, Adsorption of hydrogen on Pt(111) and Pt(100) surfaces and its role in the HOR, Electrochem. Commun. 10 (2008) 1602–1605.
4. M. Breiter,Über die art der wasserstoff adsorption an platin metall elektroden, Electrochim. Acta7 (1962) 25–38.
5. B.E. Conway, H. Angerstein-Kozlowska, W.B.A. Sharp, Temperature and pressure effects on surface processes at noble metal electrodes. Part 1.-Entropy of chemisorption of H at Pt surfaces, J. Chem. Soc., Faraday Trans. 1 74 (1978) 1373–1389.
6. P.N. Ross, Hydrogen chemisorption on Pt single crystal surfaces in acidic solutions, Surf. Sci. 102 (1982) 463–485.
7. A. Zolfaghari, G. Jerkiewicz,New findings on hydrogen and anion adsorption at a Pt(111) electrode in aqueous H_2SO_4 solution generated by temperature variation,J. Electroanal. Chem. 422 (1997) 1–6.
8. A. Zolfaghari, G. Jerkiewicz, Temperature-dependent research on Pt(111) and Pt(100) electrodes in aqueous H_2SO_4, J. Electroanal. Chem. 467 (1999) 177–185.
9. S. Mukerjee, Particle size and structural effects in platinum electrocatalysis, J. Appl. Electrochem.20 (1990) 537–548.
10. N.P. Lebedeva, M.T.M. Koper, E. Herrero, J.M. Feliu, R.A. van Santen, Cooxidation on stepped Pt[*n*(111)×(111)] electrodes, J. Electroanal. Chem. 487 (2000) 37–44.
11. J. Clavilier. K. El Achi, A. Rodes, In situ characterization of the Pt(S)-[*n*(111) x (111)] electrode surfaces using electrosorbed hydrogen for probing terrace an step sites, J. Electroanal. Chem. 272 (1989) 253–261.
12. A. Rodes, K. El Achi, M.A. Zamakhchari, J. Clavilier, Hydrogen probing of step and terrace sites on Pt(S)-[*n*(111) × (100)], J. Electroanal. Chem. 284 (1990) 245–253.
13. J. Clavilier, K. El Achi, A. Rodes, In situ probing of step and terrace sites on Pt(S)-[*n*(111) × (111)] electrodes, Chem. Phys. 141 (1990) 1–14.
14. J. Clavilier, A. Rodes, K. El Achi, M.A. Zamakhchari, Electrochemistry at platinum single crystal surfaces in acidic media: hydrogen and oxygen adsorption, J. Chim. Phys. 88 (1991) 1291–1337.
15. N.M. Markovic, T.J. Schmidt, B.N. Grgur, H.A. Gasteiger, R.J. Behm, P.N. Ross,Effect of Temperature on Surface Processes at the Pt(111)-Liquid Interface: Hydrogen Adsorption, Oxide Formation, and CO Oxidation, J. Phys. Chem. B 103 (1999) 8568–8577.

16. K. Domke, E. Herrero, A. Rodes, J.M. Feliu, Determination of the potentials of zero total charge of Pt(100) stepped surfaces in the [011] zone. Effect of the step density and anion adsorption, J. Electroanal. Chem. 552 (2003) 115–128.
17. R. Gómez, J.M. Orts, B. Alvarez-Ruiz, J.M. Feliu, Effect of Temperature on Hydrogen Adsorption on Pt(111), Pt(110), and Pt(100) Electrodes in 0.1 M $HClO_4$, J. Phys. Chem. B 108 (2004) 228–238.
18. N. García-Aráez, V. Climent, J.M. Feliu, Potential-dependent water orientation on Pt(111) stepped surfaces from laser-pulsed experiments, Electrochim. Acta 54 (2009) 966–977.
19. A. Berná, V. Climent, J.M. Feliu, New understanding of the nature of OH adsorption on Pt(1 1 1) electrodes, Electrochem. Commun. 9 (2007) 2789–2794.
20. N. Garcia-Araez, V. Climent, J.M. Feliu, Analysis of temperature effects on hydrogen and OH adsorption on Pt(111), Pt(100) and Pt(110) by means of Gibbs thermodynamics, J. Electroanal. Chem. 649 (2010) 69–82.
21. N. Garcia-Araez, Enthalpic and Entropic Effects on Hydrogen and OH Adsorption on Pt(111), Pt(100), and Pt(110) Electrodes As Evaluated by Gibbs Thermodynamics, J. Phys. Chem. C, 115 (2011) 501–510.
22. K.J.P. Schouten, M.J.T.C. van der Niet, M.T.M. Koper, Impedance spectroscopy of H and OH adsorption on stepped single-crystal platinum electrodes in alkaline and acidic media, Phys. Chem. Chem. Phys., 2010, 12, 15217–15224.
23. A. Björling, E. Herrero, J.M. Feliu, Electrochemical Oxidation of Pt(111) Vicinal Surfaces: Effects of Surface Structure and Specific Anion Adsorption, J. Phys. Chem. C 115 (2011) 15509–15515.
24. N. Garcia-Araez, V. Climent, J.M. Feliu, Temperature Effects on Platinum Single-Crystal Electrodes, Russian Journal of Electrochemistry, 48 (2012) 271–280.
25. A.M. Gómez–Marín, J. Clavilier, J.M. Feliu, Sequential Pt(111) oxide formation in perchloric acid: An electrochemical study of surface species inter-conversion, J. Electroanal. Chem.688 (2013) 360–370.
26. T. L. Hill, An Introduction to Statistical Thermodynamics, Addison-Wesley, pp. 235–241, 1960.
27. J. Clavilier, D. Armand, S. Sun, M. Petit, Electrochemical adsorption behaviour of platinum stepped surfaces in sulphuric acid solutions, J. Electroanal. Chem. 205 (1986) 267–277.
28. C. Korzeniewsky, V. Climent, J.M. Feliu, Electroanalytical Chemistry A Series of Advances Vol 24 (Eds: Bard AJ, Zoski CG) CRC Press, Boca Raton, Chap 2, pp 75–170, 2012.

29. G.A. Attard, O. Hazzazi, P.B. Wells, V. Climent, E. Herrero, J.M. Feliu, On the global and local values of the potential of zero total charge at well-defined platinum surfaces: stepped and adatom modified surfaces, J. Electroanal. Chem., 568 (2004) 329–342.

30. M.T. Koper, J.J. Lukkien, N.P. Lebedeva, J.M. Feliu, R.A. van Santen, Adsorbate interactions and phase transitions at the stepped platinum/electrolyte interface: experiment compared with Monte Carlo simulations, Surf. Sci., 478 (2001) L339–L344.

31. R. Jinnouchi, K. Kodama, Y. Morimoto, DFT calculations on H, OH and O adsorbate formations on Pt(111) and Pt(332) electrodes, J. Electroanal. Chem. 716 (2014) 31–44.

32. M.J.T.C. van der Niet, A. den Dunnen, L.B.F. Juurlink, M.T.M. Koper, Co-adsorption of O and H_2O on Nanostructured Platinum Surfaces: Does OH Form at Steps?, Angew. Chem. Int., 49 (2010) 6572–6575.

33. M. J. T. C. van der Niet, N. Garcia-Araez, J. Hernandez, J. M Feliu, M. T. M. Koper, Water dissociation on well-defined platinum surfaces: The electrochemical perspective, Cat. Today, 202 (2013) 105–113.

34. A.J. Bard, L.R. Faulkner, Electrochemical Methods: Fundamentals and Applications, 2nd ed, John Wiley and Sons, New York, 2001.

35. D. Armand, M.L. Rosinberg. A simple model for the competitive adsorption of anions and hydrogen on the (100) orientation of a platinum surface in acid medium: the three-state lattice gas model, J. Electroanal. Chem. 302 (1991) 191–206.

36. B.E. Conway, H. Angerstein-kozlowska, H.P. Dhar, On Selection of Standard States in Adsorption Isotherms, Electrochim. Acta. 19 (1974) 455–460.

37. M.J.T.C. van der Niet, I. Dominicus, M.T.M. Koper, L.B.F. Juurlink, Hydrophobic interactions between water and pre-adsorbed D on the stepped Pt(533) surface, Phys. Chem. Chem. Phys. 10 (2008) 7169–7179.

38. G.B. Fisher, J.L. Gland, The interaction of water with the Pt(111) surface, Surf. Sci. 94(1980) 446–455.

39. F.T. Wagner, T.E. Moylan, Generation of surface hydronium from water and hydrogen coadsorbed on Pt(111), Surf. Sci. 206 (1988) 187–202.

40. D. Lackey, J. Schott, J. K. Sass, S. I. Woo and F. T. Wagner, Surface-science simulation study of the electrochemical charge-transfer reaction $(H)_{ad} + (H_2O)_{ad} \rightarrow (H_3O^+)_{ad} + e^-_{metal}$ on Pt(111) and Cu(110), Chem. Phys. Lett. 184 (1991) 277–281.

41. N.G. Petrik, G.A. Kimmel, Electron-stimulated reactions in thin D_2O films on Pt(111) mediated by electron trapping, J. Chem. Phys. 121(2004) 3727–3735.

42. M.J.T.C. van der Niet, A. den Dunnen, M.T.M. Koper, L.B.F. Juurlink, Tuning Hydrophobicity of Platinum by Small Changes in Surface Morphology, Phys. Rew. Lett.107 (2011) 1461031–14610314.

43. A. den Dunnen, M.J.T.C. van der Niet, C. Badan, M.T.M. Koper, L.B.F. Juurlink, Long-range influence of steps on water adsorption on clean and D-covered Pt surfaces, Phys. Chem. Chem. Phys. 17(2015) 8530–8537.

44. A. den Dunnen, M.J.T.C. van der Niet, M.T.M. Koper, L.B.F. Juurlink, Interaction between H_2O and Preadsorbed D on the Stepped Pt(553) Surface, J. Phys. Chem. C 116 (2012) 18706−18712.

45. N. Kizhakevariam, E.M. Stuve, Coadsorption of water and hydrogen on Pt(100): formation of adsorbed hydronium ions,Surf. Sci. 275 (19929 223–236.

46. B.E. Conway, E.Gileadi,Kinetic theory of pseudo-capacitance and electrode reactions at appreciable surface coverage,Trans. Faraday Soc., 58 (1962) 2493–2509.

47. A.M. Gómez-Marín, J.P. Hernández-Ortíz,Langmuir-Hinshelwood mechanism including lateral interactions and species diffusion for CO oxidation on metallic surfaces. J. Phys. Chem. C 118 (2014) 2475–2486.

48. B. Poelsema, K. Lenzand G. Comsa, The dissociative adsorption of hydrogen on defect-'free' Pt(111), J. Phys.: Condens. Matter 22 (2010) 304006–304015.

49. B.J.J. Koeleman, S.T. de Zwart, A. L. Boers, B. Poelsema, L.K. Verheij, Adsorption Study of Hydrogen on a Stepped Pt(997) Surface using low energy recoil Scattering, Nucl. Instrum. Methods Phys. Res. 218 (1983) 225–229.

50. L. Árnadóttir, E. M. Stuve, H. Jónsson, Adsorption of water monomer and clusters on platinum(111) terrace and related steps and kinks I. Configurations, energies, and hydrogen bonding, Surf. Sci. 604 (2010) 1978–1986.

51. M.L. Grecea, E.H.G. Backus, B. Riedmuller, A. Eichler, A.W. Kleyn, M. Bonn, The Interaction of Water with the Pt(533) Surface, J. Phys. Chem. B 108 (2004) 12575–12582.

52. M.J.T.C. van der Niet, A. den Dunnen, L. B. F. Juurlink, M.T.M. Koper, The influence of step geometry on the desorption characteristics of O_2, D_2, and H_2O from stepped Pt surfaces, J. Chem. Phys. 132(2010) 1747051–1747058.

53. I. Hamada, Y. Morikawa, Density-Functional Analysis of Hydrogen on Pt(111): Electric Field, Solvent, and Coverage Effects, J. Phys. Chem. C112 (2008) 10889–10898.

54. M.J. Kolb, F. Calle-Vallejo, L.B.F. Juurlink, M.T.M. Koper, Density functional theory study of adsorption of H_2O, H, O, and OH on stepped platinum surfaces, J. Chem. Phys.140 (2014) 1347081–1347086.

55. R.A. Olsen, Ş.C. Bădescu, S.C. Ying, E.J. Baerends, Adsorption and diffusion on a stepped surface: Atomic hydrogen on Pt(211), J. Chem. Phys. 120 (2004), 11852–11863.

56. G.S. Karlberg, G.Wahnstrom, Density-Functional Based Modeling of the Intermediate in the Water Production Reaction on Pt(111), Phys. Rev. Lett. 92 (2004) 1361031–1361034.